Monthly Notices
of the
ROYAL ASTRONOMICAL SOCIETY

Mon. Not. R. Astron. Soc. **416,** 393–402 (2011) doi:10.1111/j.1365-2966.2011.19044.x

The tidal tails of NGC 2298

Eduardo Balbinot,[1,2]★ Basílio X. Santiago,[1,2] Luiz N. da Costa,[2,3] Martin Makler[2,4] and Marcio A. G. Maia[2,3]

[1]*Departamento de Astronomia, Universidade Federal do Rio Grande do Sul, Av. Bento Gonçalves 9500, Porto Alegre, RS 91501-970, Brazil*
[2]*Laboratório Interinstitucional de e-Astronomia - LIneA, Rua Gal. José Cristino 77, Rio de Janeiro, RJ 20921-400, Brazil*
[3]*Observatório Nacional, Rua Gal. José Cristino 77, Rio de Janeiro, RJ 22460-040, Brazil*
[4]*Centro Brasileiro de Pesquisas Físicas, Rua Dr. Xavier Sigaud 150, Rio de Janeiro, RJ 22290-180, Brazil*

Accepted 2011 May 10. Received 2011 May 9; in original form 2011 March 28

ABSTRACT

We present an implementation of the matched-filter technique to detect tidal tails of globular clusters. The method was tested using the Sloan Digital Sky Survey (SDSS) data for the globular cluster Palomar 5 revealing its well-known tidal tails. We also ran a simulation of a globular cluster with a tidal tail where we successfully recover the tails for a cluster at the same position and with the same characteristics of NGC 2298. Based on the simulation we estimate that the matched-filter increases the contrast of the tail relative to the background of stars by a factor of 2.5 for the case of NGC 2298. We also present the photometry of the globular cluster NGC 2298 using the MOSAIC2 camera installed on the Cerro Tololo International Observatory (CTIO) 4-m telescope. The photometry covers $\sim$3 deg^2 reaching $V \sim 23$. A fit of a King profile to the radial density profile of NGC 2298 shows that this cluster has a tidal radius of 15.91 ± 1.07 arcmin which is twice as in the literature. The application of the matched-filter to NGC 2298 reveals several extra-tidal structures, including a leading and trailing tail. We also find that NGC 2298 has extra-tidal structures stretching towards and against the Galactic disc, suggesting strong tidal interaction. Finally, we assess how the matched-filter performs when applied to a globular cluster with and without mass segregation taken into account. We find that disregarding the effects of mass segregation may significantly reduce the detection limit of the matched-filter.

Key words: globular clusters: general – globular clusters: individual: NGC 2298 – Galaxy: structure.

1 INTRODUCTION

Globular clusters (GCs) are the oldest objects found in our Galaxy. Hence they witnessed the early formation of the Milky Way (MW). Throughout the existence of a cluster, it loses stars by a series of both internal and external dynamical processes. To understand how stars formed inside a star cluster are delivered to the host galaxy is to understand a major part of the galaxy formation process in the hierarchical assembly paradigm. In that sense, the GCs that we see today are the reminiscent of a much larger population of building blocks of our Galaxy.

A GC may lose stars by a number of processes. Their internal dynamics, ruled by two-body relaxation, make stars gradually leave the cluster and lead to their eventual dissolution in a time-scale of a few hundred relaxation times (Binney & Tremaine 1987). The external influence of the gravitational field of the Galaxy may accelerate the dissolution process (Spitzer & Thuan 1972). The external field has strong effects over the overall structure of the clusters. One of the most clear evidence of this influence is the existence of a limiting radius (King et al. 1968; Trager et al. 1995). Baumgardt & Makino (2003) showed that the presence of a tidal field throughout the evolution of a cluster results in dramatic changes in the mass function. This phenomenon was latter observed on several clusters (Andreuzzi et al. 2001; De Marchi & Pulone 2007; Balbinot et al. 2009) and is associated with clusters that are subject to extreme tidal interactions.

While orbiting the host galaxy, a GC experiences a slowly varying external potential, which has little effect on its structure, except when crossing the disc or bulge of the galaxy. On the crossing event the GC potential is rapidly changed, shrinking the tidal radius in a time-scale shorter than the cluster dynamical time, rapidly turning bound stars into unbound ones. This creates a preferential way of escape along the line of action of the tidal forces. Stars that leave through the inside of the GC orbit will leap forward in the cluster path and stars on the outside will lag behind in the orbit. Since the velocity dispersion of the stars in the cluster is much less than the orbital velocity of the cluster, the stars that become loose follow

★E-mail: balbinot@if.ufrgs.br

approximately the same orbit. We may think of each unbound star as a test particle for the gravitational potential of the MW. Thus, by finding which orbit solution best fits the observed tail distribution, we may infer the best model for the MW potential (Koposov, Rix & Hogg 2010).

The study of tidal tails necessarily requires a photometrically homogeneous data set of a large number of stars to the faintest magnitudes possible. There were attempts to find tidal structures on several clusters using photographic plates (Leon, Meylan & Combes 2000), finding only mild evidence of tidal structures in 20 GCs. More crucial to tidal tails analyses is the need of a large enough solid angle, since the tails may extend over tens of degrees on the sky. With the release of the Sloan Digital Sky Survey (SDSS; York et al. 2000), it was possible to investigate large areas of the sky with deep and accurate photometry. The SDSS led to many discoveries such as tidal streams from disrupting satellite galaxies (Koposov et al. 2010), new satellite galaxies (Koposov et al. 2008; Walsh, Willman & Jerjen 2009) and tidal tails around GCs (Rockosi et al. 2002; Odenkirchen et al. 2003; Grillmair & Johnson 2006).

New large area photometric surveys are being planned for the near future. Among them is The Dark Energy Survey (DES). DES is a 5000 $\deg^2$ photometric survey that will cover the southern galactic cap in five filters (*grizY*) (DePoy et al. 2008; Mohr et al. 2008). To achieve this area coverage DES will use a large field-of-view (FOV) camera with an array of 64 high near infrared efficient CCDs. This new instrument will be placed at the Cerro Tololo International Observatory (CTIO) Blanco 4-m telescope. DES will reach fainter magnitudes than SDSS with comparable area coverage. Although its primary goal is the determination of cosmological model parameters, a by-product of DES will be the sampling of stars from our Galaxy, which may have great impact over stellar population and Galactic structure studies (Rossetto et al. 2011).

In this paper, we develop and validate an implementation of the matched-filter (MF) technique to detect sparse simple stellar populations (SSPs), such as GC tidal tails. We perform the validation on two controlled scenarios: (i) realistic simulated GC plus a tidal tail; (ii) the halo GC Palomar 5, which has a previously detected tidal tail. We then apply the algorithm to detect tidal structures on the halo GC NGC 2298 which is believed to be a cluster on advanced stages of dissolution (De Marchi & Pulone 2007). Our ultimate goal is to apply the code that we present here to the entire DES sample and, as a consequence, obtain a homogeneous sample of such tidal features across the southern sky. In Section 2 we describe the MF method. In Section 3 we present the validation tests. In Section 4 we present the NGC 2298 data reduction and the analysis of its structure and tail. In Section 5 we address the impact of mass segregation over the recovered tail from the MF. In Section 6 we present our final discussion and conclusions.

2 MATCHED FILTER

The MF is a long used technique developed for signal processing (Wiener 1949). The MF technique has a wide field of applications in astrophysics going from the detection of clusters of galaxies (Kepner et al. 1999) to the characterization of light curves of stars with eclipsing exoplanets (Doyle et al. 2000).

In this work, the MF is used to detect low-density SSPs that are projected against the Galactic field stars. This is done by determining the surface density of stars that are consistent with a given SSP by means of a weighted least-squares fit to a carefully constructed model. The implementations of the MF follow closely the work of Rockosi et al. (2002) and Odenkirchen et al. (2003). Although the MF has been well developed in these previous works, in this work we judge it necessary to redescribe the method in face of some additional features that we propose, which depend on the very definition of the functions and models adopted.

We want to detect an SSP overlaid with the Galaxy field populations. A simple model for the number of stars at a given position (α, δ) as a function of colour (c) and magnitude (m) may be written as

$$N(\alpha, \delta, c, m) = n_{\rm cl} + n_{\rm bg} \quad (1)$$

where $n_{\rm cl}$ is the number of stars belonging the SSP and $n_{\rm bg}$ is the number of Galaxy field stars. $n_{\rm cl}$ can be obtained both from observational data or from simulations using known properties of this SSP (age, metallicity, redenning, distance, mass function, unresolved binary fraction and photometric errors).

$n_{\rm cl}$ may be normalized by the total number of stars that contribute to the SSP:

$$n_{\rm cl}(\alpha, \delta, c, m) = \zeta_{\rm cl}(\alpha, \delta) f_{\rm cl}(\alpha, \delta, c, m), \quad (2)$$

where $f_{\rm cl}$ may be thought of as a probability function as in common statistics. In essence, $f_{\rm cl}$ describes the probability of randomly drawing a star from the SSP at a given colour and magnitude.

The same procedure may be applied to $n_{\rm bg}$.

$$n_{\rm bg}(\alpha, \delta, c, m) = \zeta_{\rm bg}(\alpha, \delta) f_{\rm bg}(\alpha, \delta, c, m). \quad (3)$$

A simple assumption here is to consider $f_{\rm cl}$ constant across all analysed field. This assumption bears some approximations with it. One of them is to consider the SSP at the same distance everywhere. Often, the tail extends through *kpc* scales, which may lead to variations on the distance modulus with position on the sky. A further approximation is to assume that the Present Day Mass Function (PDMF) from the cluster is the same as in the tidal tail. Baumgardt & Makino (2003) showed that dynamically evolved GCs have a rapidly evolving stellar mass function. So, the stars that are left along the tail may not be well described by the cluster PDMF, since these stars left the cluster in the past in an epoch when the mass function was different. This issue is further aggravated by mass segregation, since stars that leave the cluster are near its tidal radii, thus having a lower mass than the bulk of stars (Koch et al. 2004). In this work, we initially drop the spatial dependency of $f_{\rm cl}$, leaving an assessment of the impact caused by mass segregation to Section 5.

The number of Galaxy field stars is expected to vary slowly on large scales. This variation should be reflected on a position dependency on $f_{\rm bg}$. The scale of the analysed field and its complexity will determine if the spatial dependence of $f_{\rm bg}$ may be disregarded or not. At each case a prescription of how the spatial variability was dealt with will be presented.

Considering all approximations quoted above, we are left with a simple model for the number of stars as a function of position, colour and magnitude. This model assumes that there are only two stellar populations, the SSP itself and field stars from the Galaxy.

$$N(\alpha, \delta, c, m) = \zeta_{\rm cl}(\alpha, \delta) f_{\rm cl}(c, m) + \zeta_{\rm bg}(\alpha, \delta) f_{\rm bg}(\alpha, \delta, c, m). \quad (4)$$

The construction of $f_{\rm cl}$ and $f_{\rm bg}$ is done by means of a Hess diagram, where we divide the colour–magnitude diagram (CMD) in bins of 0.01 in colour and 0.1 in magnitude. The resulting diagram is then smoothed using a Gaussian kernel. We label the CMD bins by the index j. The sky is also divided in bins of right ascension and declination and labelled by the index i. For instance, $f_{\rm bg}(\alpha_i, \delta_i, c_j, m_j)$ is the measure of $f_{\rm bg}$ at the ith bin of spatial coordinates and the jth CMD bin. From here on we use the notation $f_{\rm bg}(i, j)$ for simplicity. Since these functions are now discrete functions of

coordinates and CMD position, we must work with new discrete functions that are integrals over the CMD and solid angle bins. The discrete model for the number of stars is

$$N(i,\,j) = \gamma_{\rm cl}(i)F_{\rm cl}(j) + \gamma_{\rm bg}(i)F_{\rm bg}(i,\,j) \quad (5)$$

where

$$\gamma_{\rm cl,bg}(i) = \int_{\Omega_i} \zeta_{\rm cl,bg}{\rm d}\Omega$$

$$F_{\rm cl}(j) = \int_{P_j} f_{\rm cl}{\rm d}m\,{\rm d}c$$

$$F_{\rm bg}(i,\,j) = \int_{\Omega_i}\int_{P_j} f_{\rm bg}{\rm d}m\,{\rm d}c\,{\rm d}\Omega,$$

where P_j is the area of the jth pixel in the CMD and Ω_i is the solid angle covered by the ith spatial bin.

Using this model for the number of stars in any region of the sky, we may now use an observed stellar sample and find the best fit to this model by means of a lest-squares fit. Let $n(i, j)$ be the observed distribution of stars. At the ith position bin the quantity to be minimized is

$$S^2(i) = \sum_j \frac{[n(i,\,j) - \gamma_{\rm cl}(i)F_{\rm cl}(j) - \gamma_{\rm bg}(i)F_{\rm bg}(i,\,j)]^2}{\gamma_{\rm bg}(i)F_{\rm bg}(i,\,j)}. \quad (6)$$

Minimizing equation (6) and solving for $\gamma_{\rm cl}$ (i.e. $\frac{{\rm d}S^2}{{\rm d}\gamma_{\rm cl}} = 0$) we have

$$\gamma_{\rm cl}(i) = \frac{\sum_j n(i,\,j)F_{\rm cl}(j)/F_{\rm bg}(i,\,j)}{\sum_j F_{\rm cl}^2(j)/F_{\rm bg}(i,\,j)} - \frac{\gamma_{\rm bg}(i)}{\sum_j F_{\rm cl}^2(j)/F_{\rm bg}(i,\,j)}. \quad (7)$$

In summary, one must plug in $n(i, j)$ in equation (7) to find the best estimate of $\gamma_{\rm cl}$, which is in turn the best estimate of the number of stars that are consistent with the SSP. Equation (7) differs slightly from that found by Rockosi et al. (2002), although it matches exactly the one found by Odenkirchen et al. (2003). This discrepancy may be due to distinct definitions and model constructions.

Note that in equation (7) the denominator for both terms is constant at every position if we neglect the spatial dependency of $F_{\rm bg}$ (i.e. no i dependency). The number of background stars ($\gamma_{\rm bg}$) can then be easily estimated from a polynomial fit to regions where we know for sure that there is no contribution from the SSP.

Our implementation of the MF was coded mostly using Python, with the aid of the SciPy module for signal processing routines. Some of the heavy array manipulation was carried out with Fortran and linked to Python using F2Py, which is part of the Numpy project. Despite being written in a high-level language, our implementation does not require a great deal of computational power or time since most of the math is carried out by external routines which are written in C or Fortran (all the MF analysis was carried out in a low-end desktop machine). We expect to release a public version of the code for the community through the Brazilian DES Science Portal in the near future.

3 VALIDATION TESTS

3.1 Simulations

To properly recreate the conditions where GCs are found (i.e. projected against a background of Galaxy field stars), we must be able to simulate field stars in any given direction of the sky. In addition, we must be able to generate realistic stellar populations from any given stellar evolution model, taking into account every observational effects. To achieve these goals a variety of software had to be employed.

The simulations of the Galaxy stars was done using the TRIdimensional modeL of thE GALaxy (Trilegal[1]) by Girardi et al. (2005). The Trilegal code simulates the stellar content of the Galaxy in any direction of the sky, including contributions from the four basic structural components: thin and thick disc, bulge and halo. We refer to the original paper for further details on the code.

To simulate a GC, we use an adaptation of the code from Kerber et al. (2002). The original code simulates the CMD of a stellar population for a given stellar evolution model, also taking into account the effects of unresolved binaries and observational errors. We modified the original code in order to include positions by spreading the stars over the sky according to a given mass profile (e.g. King 1966). In addition, a tidal tail is added using a $1/r$ density decay profile (Johnston, Sigurdsson & Hernquist 1999). Finally, we allow a position-dependent PDMF in order to incorporate mass segregation effects.

We simulate a GC located at $\alpha_{J2000} = 6^{\rm h}48^{\rm m}59^{\rm s}$ and $\delta_{J2000} = -36^\circ00'02''$, which corresponds to the position of NGC 2298, analysed in Section 4. Its structure is described by a King profile with a core radius $r_{\rm c} = 0.91$ arcmin $= 2.8$ pc and a concentration parameter $c = \log(r_{\rm t}/r_{\rm c}) = 0.94$. A Padova evolutionary model (Girardi et al. 2000) was chosen with $\log({\rm age(yr)}) = 10.10$ and [Fe/H] $= -1.98$. The simulated cluster is placed 10.8 kpc away from the Sun with no reddening for simplicity. We adopt a Kroupa IMF and choose not to include mass segregation. The adopted fraction of binaries for this simulation is of 50 per cent. The tidal tails extend 1 kpc in each direction, with a position angle of 45° and an angle with the plane of the sky of 20°. The chosen tidal tail's width is 16 arcmin $= 50$ pc. The simulated GC has $\sim 2\,10^4$ stars with 20 per cent of them belonging to the tidal tail. The simulation was carried out using the g and r passbands from DES.

A 20 deg^2 region of the Galaxy field stars was simulated using Trilegal. These stars were uniformly spread in a 24 deg^2 region around the simulated star cluster.

Photometric errors were added based on SDSS r magnitudes, which is consistent with a photometric detection limit of $r \sim 23.0$. This limit is also consistent with the observations of NGC 2298 (see Section 4.1 for details).

Since we know a priori which stars belong to the simulated cluster, it is fairly easy to build $F_{\rm cl}$; the same is true for $F_{\rm bg}$. We applied the MF to four tidal tails with different densities, 20 per cent (3200), 10 per cent (1600), 5 per cent (800) and 1 per cent (160) of the total number of simulated cluster stars. This was done by randomly removing stars from the simulated tail. Furthermore, we compared the MF results with a simpler method of quantifying the simulated tidal tail, based on simple star counts. In this alternative method we compute star counts at each spatial bin, evaluate the expected average background counts and subtract this later from the former.

Fig. 1 shows the on-sky distribution of simulated stars compared to the MF results. It is clear that the MF improves the contrast of the tail relative to the field stars when compared to a direct star counting method. Yet, the comparison of the left- and right-hand columns in the figure reveals that the MF does not recover all the structure and extension in the tails, especially in the sparser cases. In Fig. 2 we compare, for the two methods, the resulting cluster counts to the actual number of simulated cluster stars. The MF clearly reduces the noise in this scatter plot by a factor of 1.92/0.72 = 2.67, and therefore the contrast with the background, when compared to the

[1] http://stev.oapd.inaf.it/trilegal

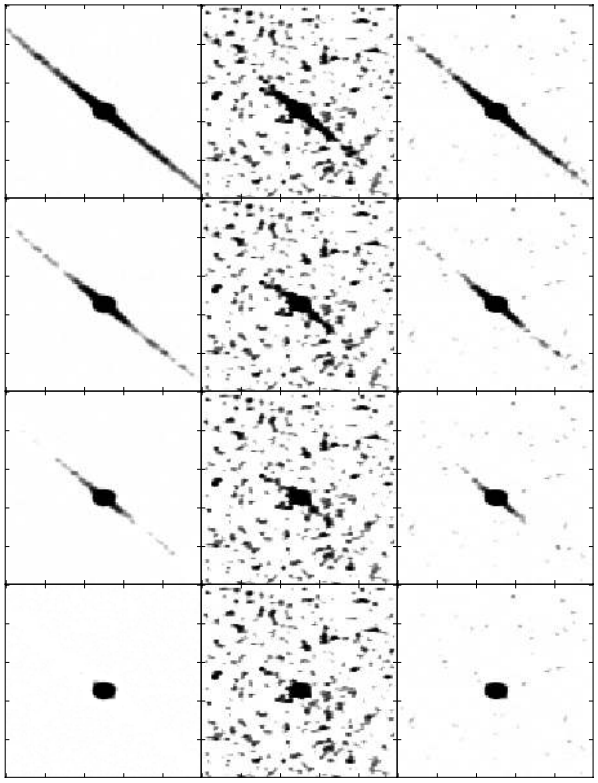

Figure 1. Output of the simulations. Each panel covers 6° by 4° on the sky. The left-hand column shows the number of simulated cluster and tail stars. The central column shows the total number of simulated stars, cluster, tail and field, after subtraction of the average number over the entire simulation field (star counts method). The right-hand column shows the output of the MF, $\gamma_{\rm cl}$, as described in Section 2.

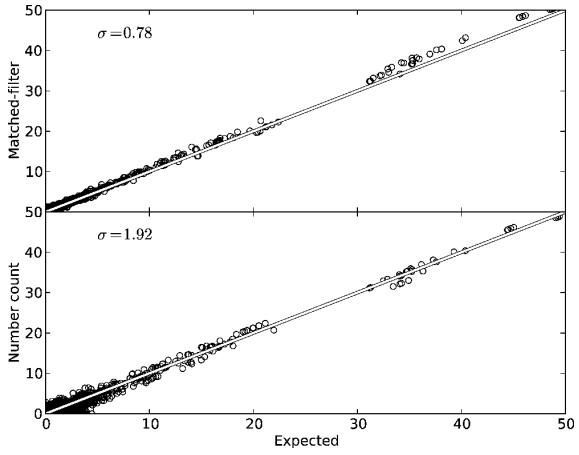

Figure 2. Comparison between the simulated number of cluster stars (in the *x*-axis) with the number derived from simple number counts (lower panel) and from the MF (upper panel). The identity line is shown in both panels. The dispersion is also indicated in the top-left corner of each panel.

simple star counts method. We conclude that the our implementation of the MF works well for this simulated set.

3.2 Palomar 5

In order to further validate our algorithm we have chosen the halo GC Palomar 5. This cluster has the most prominent tidal tail known to date, making it a good test case for any detection algorithm.

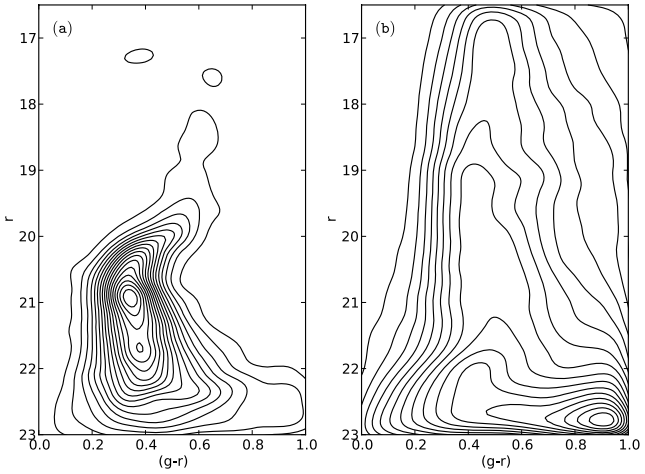

Figure 3. Panel (a): r, $(g - r)$ $F_{\rm cl}$ contours on the CMD plane for the Palomar 5 SDSS data. Panel (b): same as in panel (a) but now showing the $F_{\rm bg}$ contours. In both panels the contour levels are normalized to the range varying from 0 to 1, and are evenly spaced by 1/20.

Our analysis was carried out using the SDSS Data Release 7 (DR7) (Abazajian et al. 2009). SDSS is a large survey, covering up to 10 000 deg^2 of the northern and part of the southern galactic cap, using five filters (*ugriz*). Its large continuous area coverage and photometric homogeneity make it a very useful data set for the discovery of tidal tails or any other large-scale sub-structure in the Galaxy.

Although SDSS reaches r magnitudes up to 23.5, we avoid stars fainter than 22.5. This conservative limit is set to avoid any complications due to misclassification of stars and galaxies.

$F_{\rm cl}$ was built using a circular region around the centre of Palomar 5 with a 0.°13 radius. Fig. 3(a) shows the $r \times (g - r)$ Hess diagram constructed using the stars located inside this circular region. Some of the expected features of a typical GC are visible: a main-sequence (MS), MS turn-off (MSTO), red giant branch (RGB) and horizontal branch (HB). The choice of contour levels of Fig. 3 is such that the asymptotic giant branch (AGB) and the blue stragglers (BS) are not visible despite being present in this cluster. To avoid minor contributions of background stars in the region where $F_{\rm cl}$ was built, we only used stars that occupy the loci expected for a GC population.

As discussed in previous sections, $F_{\rm bg}$ is expected to vary over large scales. To accommodate some of this variation, we follow the prescriptions of Rockosi et al. (2002) and take the average Hess diagram of four 3 deg^2 fields far away from Palomar 5. The fields used are centred in the same coordinates as in Rockosi et al. (2002). The resulting Hess diagram is shown in Fig. 3(b). This approach to the construction of $F_{\rm bg}$ is such that the spatial dependency should be reduced, hence simplifying the solution of equation (7). We thus apply the MF under the assumption that the background term does not vary with position. The measured background is of 0.51 arcmin^{-2}. Fig. 4 shows the smoothed (0.°1 Gaussian smoothing) distribution of stars consistent with Palomar 5 stellar population.

Having $F_{\rm cl}$ and $F_{\rm bg}$ properly constructed, we may retrieve the best estimate of the density of stars consistent with $F_{\rm cl}$ in any region of the sky where $F_{\rm bg}$ well describes the Galaxy field star population. We applied the MF to a region $226° < {\rm RA} < 231°$ and $-1.°1 < {\rm Dec.} < 1.°1$, which was divided in a grid of $0.°03 \times 0.°03$ bins. Fig. 4 shows the results of the MF as a stellar surface density of Palomar

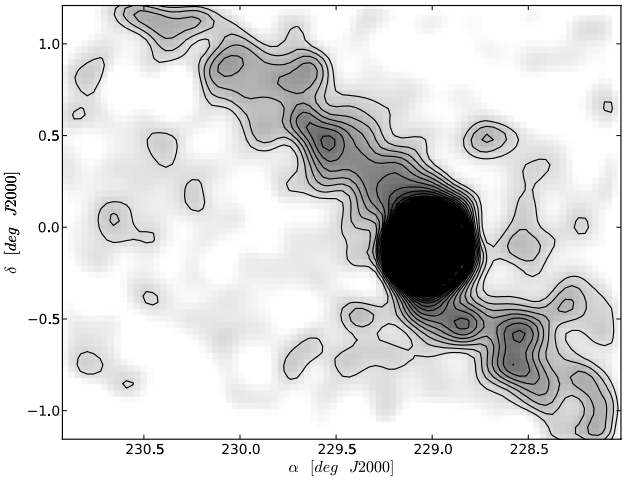

Figure 4. The stellar number density map resulting from the MF applied to SDSS data around Palomar 5. We show the number of stars in grey-scale. The contour map emphasizes the more populated regions. The four outermost contours correspond to 0.1, 0.15, 0.20, 0.25 star arcmin^{-2}. Near the centre of Palomar 5 we do not show any contour for clarity.

5 like stars overlaid on a residual contribution by background stars (i.e. the last term in equation 7).

The extra-tidal structure recovered for Palomar 5 closely resembles the one found in previous works using the MF technique. The peak of density along the tail is expected to be of $\sim$0.2 arcmin^{-2} according to Odenkirchen et al. (2003). In this work we find a maximum density of $\sim$0.27 arcmin^{-2} using a different set of colours and magnitudes.

The recovered Palomar 5 tail extends throughout 1.°8, ending at the edge of the analysed field, which suggests a tail that extends much further, as depicted by Odenkirchen et al. (2003). Several density fluctuations are found along the tail. Most of these were also found in these previous studies. The fluctuations are expected even for the simplest of the orbits such as circular orbits on a axisymmetric potential (Küpper, MacLeod & Heggie 2008; Küpper et al. 2010).

4 NGC 2298

NGC 2298 (also designated by ESO 366-SC 022) is located at $l = 245.°63$, $b = -16.°01$, and therefore projected towards the Galactic anti-centre. Its position places it near the Galactic disc. It is thus superimposed on to the thin and thick discs, besides the halo. Structural parameters were found by De Marchi & Pulone (2007), such as core radius $r_c = 0.29$ arcmin and tidal radius $r_t = 8.0$ arcmin leading to a concentration parameter of $c = \log(r_t/r_c) = 1.44$. The distance and metallicity taken from Harris (1996) are $d = 10.80$ kpc and [Fe/H] $= -1.85$. The analysis of the *Hubble Space Telescope* (*HST*)/Advanced Camera for Surveys (ACS) CMD from those authors also yielded an extinction of $E(B - V) = 0.15$ towards the cluster.

We here describe a first attempt to detect an extra-tidal structure around NGC 2298, using a field of $\simeq$4 deg^2 around the cluster. Its location towards a dense stellar field, with likely varying extinction, makes it a harsher test of the MF method that we implemented. NGC 2298 is one of the GCs located in the footprint of DES. Therefore, DES will provide a much larger area coverage around the cluster, making it possible to do undertake follow-up studies using the same methods developed for this paper.

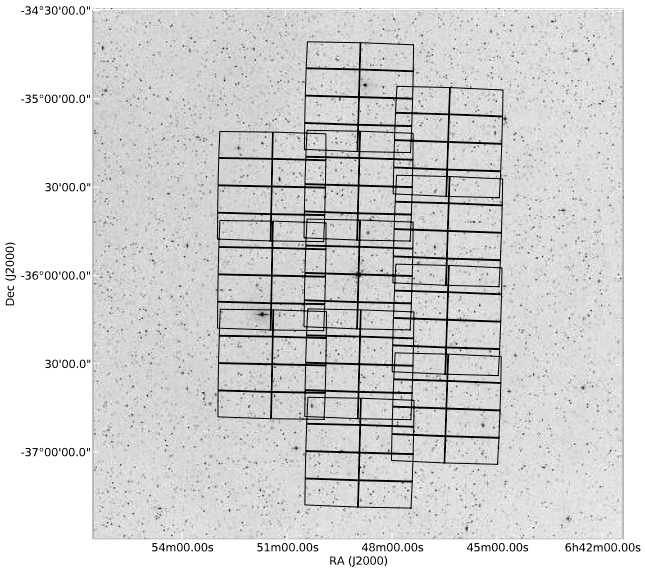

Figure 5. 3° × 3° DSS *r*-band image with the borders of the 12 observed MOSAIC2 FOV overlaid in red. Note the complex shapes introduced by the gaps between the CCDs.

4.1 Data

NGC 2298 was observed using the MOSAIC2 camera located at the 4-m Blanco Telescope at CTIO. The MOSAIC2 instrument is a 8192 × 8192 pixel segmented CCD camera with a FOV of 36 × 36 arcmin. Each of the eight camera segments is a CCD with 4096 × 2048 pixel. Separating each CCD there is a gap of 35 pixel = 9.2 arcsec in the east–west direction and 50 pixel = 13.2 arcsec in the north–south direction. The wide field of MOSAIC2 makes it the best instrument for large area observations in the Southern hemisphere.

The observations took place in the night of 2010 February 10 under photometric conditions. The mean seeing for the night was 0.7 arcsec, which is normal for the epoch. We observed 12 overlapping fields around NGC 2298 in two passbands, *V* and *I*. Fig. 5 shows the fields and their CCD segments overlaid on a Digital Sky Survey (DSS) image around the cluster. The fields in the figure have been corrected for geometric distortions, as explained latter. The total exposure time was of 240 s (2 × 120 s) in the *V* band and 360 s (3*x*120 s) in the *I* band. The standard stars used for photometric calibration are taken from Stetson (2000). They are located within 30 arcmin of the cluster centre and were observed several times during the night, each time using one single short exposure in the *V* and *I* bands. MOSAIC2 was set to 1 × 1 binning on the eight-channel mode.

The reduction of the data was carried out using the MSCRED package running on the IRAF environment. All frames were reduced using standard procedures (crosstalk, overscan, bias, flat-field). Some complications arise when dealing with large field instruments. The FOV of MOSAIC2 introduces a spatial variation on the pixel size going from 0.27 arcsec pixel^{-1} in the centre of the FOV to 0.29 arcsec pixel^{-1} on the edges. This means that each exposure from a given field must be corrected for distortion before being stacked, since the projection depends on the pointing of the telescope. To correct for distortion each frame must have a reasonably accurate astrometric solution. This was done by constructing an initial guess for the World Coordinate System (WCS). This initial

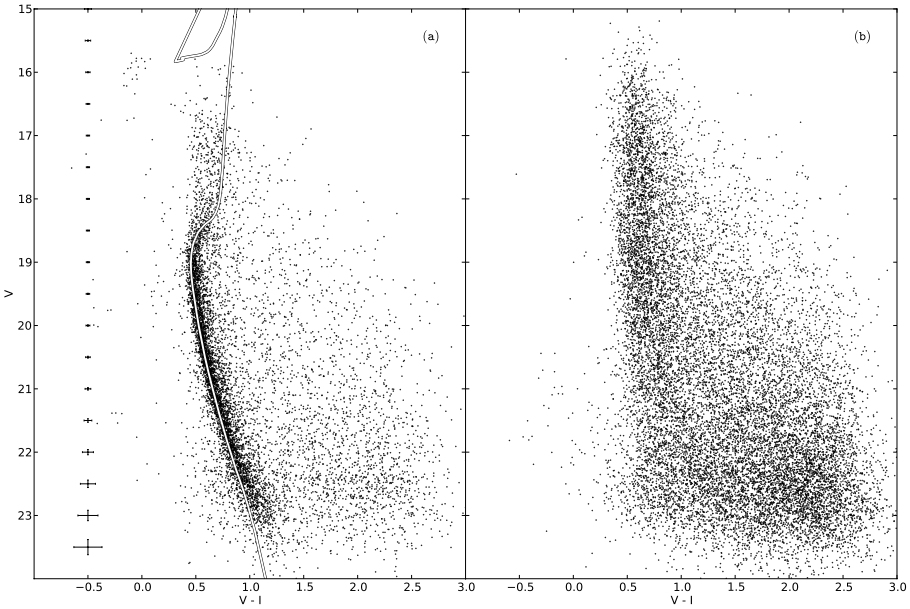

Figure 6. Panel (a): V, $(V - I)$ CMD of NGC 2298 where only stars inside $r = 37$ pc where chosen. The mean photometric error is shown in the extreme left of this panel. We also show the best-fitting isochrone with $(m - M) = 15.15$ and the $(V - I)$ offset of 0.06 explained in the text. Panel (b): V, $(V - I)$ CMD for stars outside $r = 37$ pc. Only 10 per cent of the total stars are shown for clarity.

guess was determined using USNO-A catalogues.[2] With the initial guess for the WCS, we refine the astrometric solution frame by frame using the task MSCCMATCH. Frames that will be later combined are registered using MSCIMATCH and, finally, using the task MSCIMAGE, all frames were corrected for distortions and combined into a single image. Since the process of distortion correction involves a re-sampling of the pixels, the bad pixel areas suffer distortions in the process due to the artificial step discontinuity in the image. To overcome this problem, the bad pixel masks were also corrected for distortions and later applied to the final combined image.

4.2 Photometry

With the final combined images we performed point spread function (PSF) fit photometry using the broadly used DAOPHOT software (Stetson 1994). All the photometry was performed by an automated python script. The script deals with each of the eight MOSAIC2 chips independently since there may be PSF variations from one chip to another. The list below shows the steps taken to accomplish the photometry for each chip.

(1) Find sources above $4\sigma_{\rm sky}$ (DAOFIND).
(2) Run aperture photometry (PHOT).
(3) Construct the PSF model using bright non-saturated and isolated stars.
(4) Fit the PSF model for each source (ALLSTAR).
(5) Transform from physical to world coordinates.

In addition, the PSF was allowed to vary over each chip to account for any residual distortions. After this process, we combined the photometric tables from the two filters using a positional matching in world coordinates.

[2] Made available to the community at http://www.ctio.noao.edu/mosaic/

The combined VI photometric table for each field was calibrated using the following calibration equations:

$$V = v + a(V - I) + bX + v_0$$

$$I = i + c(V - I) + dX + i_0,$$

where $V(I)$ is the calibrated magnitude, $v(i)$ is the instrumental magnitude, $(V - I)$ is the calibrated colour, X is the airmass and v_0 (i_0) is the zero-point. The coefficients (a, b, c, d), as well as the zero-points, were obtained from a fit to the magnitudes and colours of the standard stars observed during the night with air-masses ranging from 1.01 to 2.60.

The final step to the data reduction is to apply aperture corrections. These corrections are necessary since there may be *seeing* variations from field to field. The aperture corrections were determined using the overlapping regions on adjacent fields, starting by the central pointing, which contains the cluster and the standard stars.

To eliminate spurious detections, and possibly galaxies, we performed a cut in the magnitude error of the final photometric table. This cut eliminates sources with errors larger than those expected for point sources at their magnitude value. This process eliminates most spurious detections including many galaxies that could introduce uncertainties to the tidal tail detection.

The final photometric sample has approximately 152 000 stars. The mean photometric error in the range $16 \leq V \leq 22$ is less than 0.05, which is enough for our purposes. All magnitudes were corrected for extinction using Schlegel, Finkbeiner & Marc (1998) dust maps. The mean reddening for the entire observed region is $E(B - V) = 0.20$.

In Fig. 6(a) we show the CMD for the stars within 12 arcmin $= \sim 37$ pc, which corresponds to 1.5 tidal radius as quoted by De Marchi & Pulone (2007). The structure of the CMD is typical of an old metal-poor GC. Note that at bright magnitudes we lose stars due to saturation, although the blue end of the extended HB is still visible. Larger errors on brighter magnitudes are due to saturation in the I band. In Fig. 6(b) we show the CMD for stars outside 12

arcmin; in this plot we choose to display only a fraction of 10 per cent of the total number of points for clarity.

Using the best determination of NGC 2298 age and metallicity (De Marchi & Pulone 2007), we overlay the corresponding Padova isochrone to the data in Fig. 6(a). The best fit occurs for a distance modulus of $(m - M) = 15.15$, which closely agrees with the estimate from Harris (1996). However, a $(V - I)$ offset of 0.06 towards blue colours was applied to properly fit the isochrone to the MS and MSTO. This offset reflects the discrepancy between the reddening value from the Schlegel et al. (1998) dust maps, $E(B - V) = 0.20$, and that found by De Marchi & Pulone (2007). In what follows, for the sake of coherence, we use the Schlegel et al. (1998) values over the entire field covered by our MOSAIC2 data.

For completeness reasons we chose not to match stars in overlapping regions. All the analysis was done on a field-by-field basis and, when necessary, we adopt the proper area correction (e.g. border of the fields and chips) using a carefully constructed mask. This mask also takes bad pixel regions into account when calculating any area. All areas calculated hereafter were obtained by a Monte Carlo integral and accounting for the mask we built (see Balbinot et al. 2009 for further details).

4.3 Cluster structure

To make an independent measurement of NGC 2298 structural parameters we built its radial density profile (RDP). The RDP was built by counting stars in radial bins out to the point where the background is clearly reached. For the cluster centre, we simply used values given in the literature.

In Fig. 7 we show the resulting RDP for NGC 2298. We choose not to use the cluster's most central region due to incompleteness caused by both crowding and gaps on the CCD mosaic. Our RDP analysis covers out to an angular distance of 25 arcmin which corresponds to 78 pc. This is approximately three times the best estimation of tidal radius found in the literature. We fitted a King profile with fixed core radius ($r_c = 0.29$ arcmin $= 0.9$ pc) since our central densities are not accurate due to crowding. We find a larger tidal radius of $r_t = 15.91 \pm 1.07$ arcmin, which corresponds to 50 pc, which is twice larger than previously found. The background density found is $\sigma_{bg} = 9.50 \pm 0.10$ stars arcmin^{-2}.

The last time NGC 2298 was observed with such a large FOV and photometric depth was by Trager et al. (1995). The authors find a tidal radius of 6.48 arcmin although not reaching deep magnitudes. Later, De Marchi & Pulone (2007) found a tidal radius of 80 arcmin, although using only data that cover a 3.4×3.4 arcmin FOV. Hence, their estimated tidal radius relies on data that do not reach the full extension of the cluster. Our determination combines the advantages of larger depth compared to photographic plates and larger FOV compared to *HST*/ACS.

NGC 2298 was one of the first GCs to be found with a high degree of depletion of low-mass stars (De Marchi & Pulone 2007). The inverted mass function and the low concentration parameter are expected for old GCs that are subject to a high degree of tidal interactions (Baumgardt & Makino 2003).

Based on the fitted isochrone, the mass range sampled by our observation of NGC 2298 is very limited, $0.6 \leq M_{\odot} \leq 0.79$. The inner parts of NGC 2298 are not accessible to us due to crowding. On the outer parts the number of stars is too low at our photometric depth, giving low statistical significance to the mass function. We thus refrain from making a PDMF reconstruction with our CTIO data; deeper observations covering a wider range of masses, such as those that will be provided by DES, are necessary to accurately determine the slope of the mass function in the outskirts of NGC 2298.

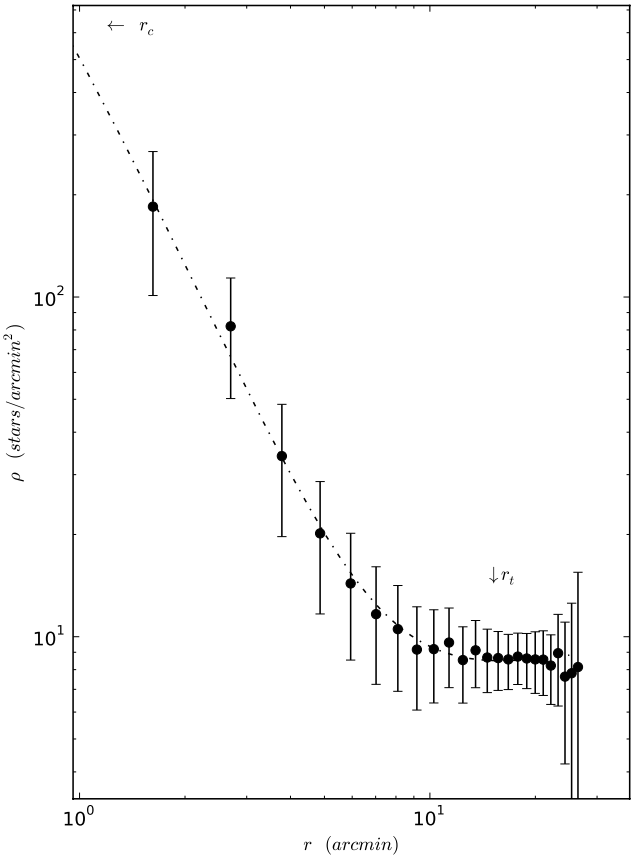

Figure 7. The logarithmic scale RDP for NGC 2298 with 1σ error bars. The dot–dashed line shows the best fit of a King profile with a core radius fixed at $r_c = 0.29$ arcmin $= 0.9$ pc, as found in the high-resolution data from De Marchi & Pulone (2007). The best-fitting values are $r_t = 15.91 \pm 1.07$ arcmin with a background density of $\sigma_{bg} = 9.50 \pm 0.10$ stars arcmin^{-2}. The tidal and core radius positions are indicated. Note that the core radius is out of bounds in this plot.

4.4 Extra tidal structure

We follow the same MF recipe adopted for Palomar 5 in Section 2 in order to investigate the presence of tidal tails associated NGC 2298. F_{cl} was built using stars that are less than 37 pc from NGC 2298 centre. As seen in Fig. 6, a relatively large amount of field stars are present in the region chosen to build F_{cl}. These field stars were eliminated by choosing a CMD locus that is consistent with the cluster evolutionary sequence in the same fashion as in Balbinot et al. (2009). F_{bg} was built using six fields near the edges of the observed region. F_{cl} and F_{bg} were built using the completeness limit of the most crowded region. This conservative approach avoids most issues that might arise from non-homogeneous photometry.

In Fig. 8 we show the resulting star count map for NGC 2298 after applying the MF. Several features are found above the 1σ confidence level. One interpretation of our findings is that the extended northwest tail is the trailing tail since its orientation is opposed to the proper motion (Dinescu et al. 1999). The two smaller opposing structures found in the central east–west direction may be the result of the tidal interaction with the disc, since they point towards the disc and NGC 2298 is close to the Galactic plane. In addition, a faint structure appears ahead of NGC 2298's motion, which may be

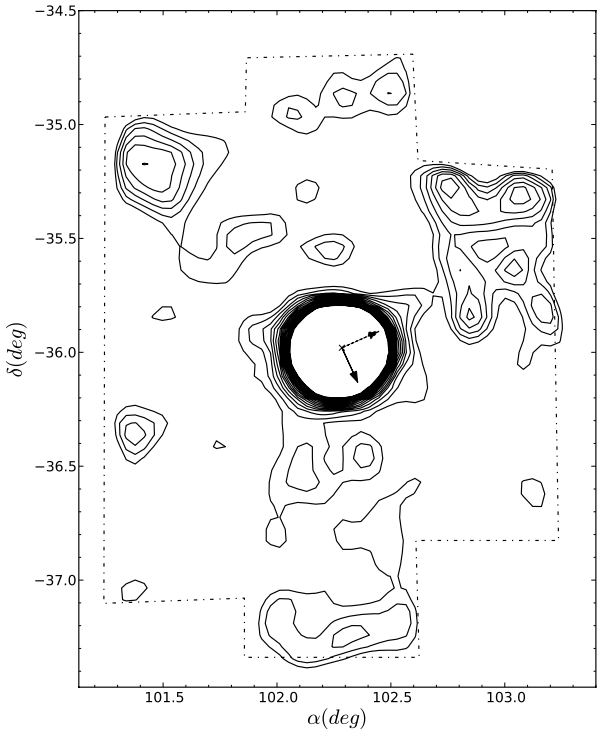

Figure 8. The result of applying the MF to NGC 2298 CTIO data. We show the derived number of stars, $\gamma_{\rm cl}$, in a contour plot. The first three contour levels correspond to 0.8, 1.8, 2.8σ above background. The inner contours start at the tidal radius of the cluster. The dashed arrow points to the direction perpendicular to the Galaxy disc. The solid line points towards the proper motion direction (Dinescu et al. 1999). The resulting map was smoothed using a $0\overset{\circ}{.}06$ Gaussian kernel, thus enhancing structures with a typical size similar to $r_{\rm t}$.

the leading tail. The two structures found at the extreme north and south most likely are boundary effect introduced by the smoothing process. At last, a strong northeast structure appears in the direction perpendicular to the Galactic disc. This may be interpreted as stars that have left the cluster although have not had time to fall behind or ahead of the orbit. Another faint structure opposite to the previous one is present, although not connected to any other enhancement.

Our findings are similar to those predicted by Combes, Leon & Meylan (1999). The authors' simulations predict a formation of multiple perpendicular tails in a cross-like pattern resulting from multiple disc crossings.

We do not discard the possibility that some of the features detected are in fact due to wrong extinction corrections. They could result from high-frequency structures on the dust filaments close to the disc. These structures are not properly sampled due to resolution limitations of the Schlegel et al. (1998) maps built using *IRAS* that has a full width at half-maximum (FWHM) = 6.1 arcmin. However, most of the structures seen in Fig. 8 extend along many *IRAS* FWHMs and thus are likely to be real.

5 EFFECTS OF MASS SEGREGATION

So far, the MF technique has been applied without any assessment of the influence of improperly built $F_{\rm cl}$. That is, if $F_{\rm cl}$ does not reflect the distribution of cluster stars in the colour–magnitude space, as well as its variations, throughout the entire FOV, the application of the MF may lead to misidentifications of tidal structures. One phenomenon that may give rise to an improper $F_{\rm cl}$ is mass segregation.

Table 1. PDMF power-law slopes for different annuli. Column 1 shows the distance range in *parsec*. Column 2 shows the simulation power-law slopes for the mass range of 0.08–0.80 $M_{\odot}$.

Distance (pc)	α
0.5	1.6
1.5	1.1
2.5	0.5
3.5	0.1
4.5	0.0
5.5	−0.1
6.5	−0.5
7.5	−1.1
8.5	−1.6
$r \leq 9.5$	−1.6

We here attempt to quantify its effect on a model cluster consistent with NGC 2298.

To assess the effect of mass segregation on the MF technique, we made another simulation of a GC similar to NGC 2298, but now using the PDMF from the literature. Since the slope of the PDMF is only determined to a distance of 1.8 arcmin, we extrapolate it to 3.6 arcmin by assuming the same growth rate of the PDMF slope as in the inner parts of NGC 2298. For the outermost parts of the cluster, we assume that the PDMF slope saturates at the value at 3.6 arcmin. This latter value, therefore, is the one that applies to most extra-tidal stars in the model. Table 1 lists the model slopes at different distances from cluster centre. We also run another simulation, which is identical to the previous one, but without mass segregation. In this second, non-segregated case, the PDMF slope used is the one corresponding to the outermost bin in Table 1.

The simulation parameters and number of simulated stars in these two extra simulations are the same as in Section 3.1, except for the PDMF slopes, as described. The background of stars is also the same one used in that section, built using TRILEGAL.

In Fig. 9, we show the comparison of the true number of cluster stars to those detected using the MF, in cases where mass segregation is present or absent. Note that there are no systematic changes in the number of stars obtained in either situation. However, there is a significant difference on the dispersion, in that the MF reconstructed star counts have larger scatter in the cluster which is subject to mass segregation. We thus conclude that, even though the detection of a tidal tail is still possible in the presence of mass segregation effects, the limiting distance out to which the tail may be detected, as well as some of its low-density substructure, may be affected if $F_{\rm cl}$ does not properly take segregation into account.

We would like to point out that another effect that was not taken into account in this work is the difference in the completeness of the sample in different regions of the FOV. For instance, the cluster core is affected by crowding, thus having a fainter completeness limit than the background stars. Using the MF without any completeness correction may lead to an incorrect surface density of stars, affecting mainly low-mass stars. One conservative way of resolving this issue is to use the completeness limit of the most crowded field for all stellar sample analysed with the MF. Another way is to run fake star experiments to properly access the completeness as a function of colour, magnitude and CCD position.

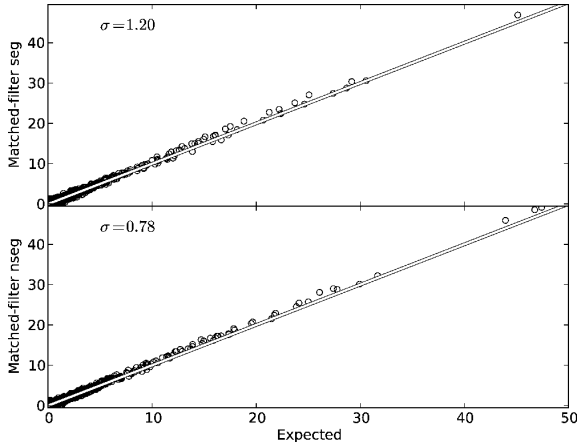

Figure 9. Comparison of the number of cluster stars detected using the MF (vertical axis) with the actual number of simulated stars (horizontal axis). The top panel shows the comparison for a mass-segregated cluster, whose PDMF slopes are listed in Table 1. The bottom panel shows the comparison for a non-segregated cluster. The identity line is shown on both panels. The dispersion in the plots is indicated at the top left.

6 DISCUSSION

We developed an implementation of the MF technique that is relatively user-independent and with great potential for being used in a large scale. These features make it suitable to be applied to deep and wide angle, such as DES, SDSS, Panoramic Survey Telescope and Rapid Response System (PanSTARSS) and Large Synoptic Survey Telescope (LSST), in a systematic way to find GC tidal tails and other MW halo sub-structures.

The MF was tested on simulated data, showing that it increases the contrast of the tail relative to the background by a factor of 2.5 for a cluster projected against a dense background, similar to that of a low-latitude GC, such as NGC 2298. The MF was also tested on a real scenario where it successfully recovered the tidal tail of Palomar 5. The Palomar 5 tail closely resembles previous detections in the literature, reproducing both shape and density.

We then study the GC NGC 2298, which is a good candidate to have a tidal tail due to its previously studied PDMF and location. We found that the cluster has a tidal radius of $r_t = 15.91 \pm 1.07$ arcmin when a King profile is fitted and keeping the core radius fixed ($r_c = 0.29$ arcmin). Our r_t value is almost twice that of previously found in the literature. It is based on deeper photometry than previous photographic work and on a much wider area than previous high-resolution and deep photometry. The new value for r_t changes the concentration parameter of NGC 2298 to $c = 1.44$, pushing it further away from the α–c relation from De Marchi et al. (2010). This discrepancy makes us wonder if the tidal radius of other clusters like NGC 6838 and NGC 6218 is not similarly affected by observational biases associated with small fields or shallow photometry. For instance, NGC 6218 has a tidal radius of 17.2 arcmin whereas observations only cover 3.4 arcmin (De Marchi, Pulone & Paresce 2006). There are no publications available for NGC 6838 to properly access if its tidal radius determination uses data that extend beyond its literature tidal radius. We point out that the determination of the tidal radius of Palomar 14 by Sollima et al. (2011) also shows an increase by a factor of 4 when compared to previous determinations in the literature. The increase of the tidal radius appears to be a trend in the sense that whenever large FOV are used, the tidal radius increases.

Applying the MF technique to NGC 2298, we find that this GC has several extra-tidal structures detected above 1σ confidence level. The strongest feature is the elongation of the cluster along the direction of the disc, suggesting strong tidal interaction. We also find what appears to be faint leading and trailing tails, both extending to the edges of the observed field ($\sim 1\overset{\circ}{.}5$). At last a large structure is found, spreading from the cluster towards the disc direction. This structure may be a halo of NGC 2298 that got ejected on the last disc crossing.

Follow up observations are necessary to properly access the nature of each extra-tidal structure found around NGC 2298. We expect DES to give this follow up. The survey is going to reach 1 mag deeper than our observations with a much larger area, better photometric calibrations and three more passbands. DES will thus allow us to analyse the extra-tidal structure of NGC 2298 in more detail and over larger distances. A larger area will also enable us to test sophistications to the SSP and background models underlying the MF, such as a varying background.

Finally, we simulate a cluster with and without mass segregation to evaluate how mass segregation affects the MF results, via an F_{cl} that does not adequately describe the CMD in the outer regions of a mass-segregated cluster. We find that there is no strong systematic effect in the reconstructed density of stars. There is, however, a significant difference in the density fluctuations relative to the truth table, in the sense that the mass-segregated cluster has a larger dispersion around the simulated densities. This is the result of its F_{cl} not being able to accommodate the variation in the CMD caused by a position-dependent PDMF. We thus conclude that the impact of unaccounted for mass segregation in the MF process is to make it more difficult to detect the full extension and the structural details of a GC tidal tail, rather than preventing the tidal tail detection per se. To the best our knowledge, this is the first time the MF was tested for an intrinsically variable and unaccounted for F_{cl}.

ACKNOWLEDGMENTS

We are grateful to the CTIO local staff for their help during observation/reduction. We acknowledge support from Conselho Nacional de Desenvolvimento Científico e Tecnológico (CNPq) in Brazil.

We also thank the support of the Laboratório Interinstitucional de e-Astronomia (LIneA) operated jointly by the Centro Brasileiro de Pesquisas Fisicas (CBPF), the Laboratório Nacional de Computação Científica (LNCC) and the Observatório Nacional (ON) and funded by the Ministry of Science and Technology (MCT)

REFERENCES

Abazajian K. N. et al., 2009, ApJS, 182, 543
Andreuzzi G., De Marchi G., Ferraro F. R., Paresce F., Pulone L., Buonanno R., 2001, A&A, 372, 851
Balbinot E., Santiago B. X., Bica E., Bonatto C., 2009, MNRAS, 396, 1596
Baumgardt H., Makino J., 2003, MNRAS, 340, 227
Binney J., Tremaine S., 1987, Galactic Dynamics. Princeton Univ. Press, Princeton, NJ
Combes F., Leon S., Meylan G., 1999, A&A, 352, 149
De Marchi G., Pulone L., 2007, A&A, 467, 107
De Marchi G., Pulone L., Paresce F., 2006, A&A, 449, 161
De Marchi G., Paresce F., Portegies Zwart S., 2010, ApJ, 718, 105
DePoy D. L. et al., 2008, in McLean I. S., Casali M. M., eds, SPIE Vol. 7014, Ground-based and Airborne Instrumentation for Astronomy II. SPIE, Bellingham, 70140E
Dinescu D. I., van Altena W. F., Girard T. M., López C. E., 1999, AJ, 117, 277

Doyle L. R. et al., 2000, ApJ, 535, 338
Girardi L., Bressan A., Bertelli G., Chiosi C., 2000, A&AS, 141, 371
Girardi L., Groenewegen M. A. T., Hatziminaoglou E., da Costa L., 2005, A&A, 436, 895
Grillmair C. J., Johnson R., 2006, ApJ, 639, L17
Harris W. E., 1996, AJ, 112, 1487
Johnston K. V., Sigurdsson S., Hernquist L., 1999, MNRAS, 302, 771
Kepner J., Fan X., Bahcall N., Gunn J., Lupton R., Xu G., 1999, ApJ, 517, 78
Kerber L., Santiago B., Castro R., Valls-Gabaud D., 2002, A&A, 390, 121
King I. R., 1966, AJ, 71, 64
King I. R., Hedemann E., Jr, Hodge S. M., White R. E., 1968, AJ, 73, 456
Koch A., Grebel E. K., Odenkirchen M., Martínez-Delgado D., Caldwell J. A. R., 2004, AJ, 128, 2274
Koposov S. et al., 2008, ApJ, 686, 279
Koposov S. E., Rix H.-W., Hogg D. W., 2010, ApJ, 712, 260
Küpper A. H. W., MacLeod A., Heggie D. C., 2008, MNRAS, 387, 1248
Küpper A. H. W., Kroupa P., Baumgardt H., Heggie D. C., 2010, MNRAS, 401, 105
Leon S., Meylan G., Combes F., 2000, A&A, 359, 907
Mohr J. J. et al., 2008, in Brissenden R. J., Silva D. R., eds, Proc. SPIE Vol. 7016, Observatory Operations: Strategies, Processes, and Systems II. SPIE, Bellingham, 70160L
Odenkirchen M. et al., 2003, AJ, 126, 2385
Rockosi C. M. et al., 2002, AJ, 124, 349
Rossetto B. M. et al., 2011, AJ, 141, 185
Schlegel D. J., Finkbeiner D. P., Davis M., 1998, ApJ, 500, 525
Sollima A., Martínez-Delgado D., Valls-Gabaud D., Peñarrubia J., 2011, ApJ, 726, 47
Spitzer L., Jr, Thuan T. X., 1972, ApJ, 175, 31
Stetson P. B., 1994, PASP, 106, 250
Stetson P. B., 2000, PASP, 112, 925
Trager S. C., King Ivan. R., Djorgovski S., 1995, AJ, 109, 218
Walsh S. M., Willman B., Jerjen H., 2009, AJ, 137, 450
Wiener N., 1949, Extrapolation, Interpolation, and Smoothing of Stationary Time Series. Tech. Press MIT, Cambridge, MA
York D. G. et al., 2000, AJ, 120, 1579

This paper has been typeset from a TEX/LATEX file prepared by the author.